shorter than the C–Se bond lengths of 1.97 Å found in the salt of **2**, causes the distortions in **1**, $n = 3$, to be quantitatively larger. For example the pyramidalization angles at the double-bonded carbons are predicted to be 30° and 33° in **1**, $n = 3$.[22] Therefore, the finding that **2** is an isolable molecule, stable at room temperature, makes the hydrocarbon (**1**, $n = 3$) an especially attractive target for synthesis and study.

Acknowledgment. We thank the National Science Foundation for support of this work.

Supplementary Material Available: Crystallographic data for the methylselenonium triflate salt of **2**—crystal data and summary of data collection and refinement, fractional coordinates and thermal parameters, anisotropic thermal parameters, interatomic distances, and interatomic angles (5 pages). Ordering information is given on any current masthead page.

(22) There is some evidence that MM2 may tend to overestimate the amount of pyramidalization in **1**, $n = 3$.[4]

Preparation and Characterization of Molecule-Based Transistors with a 50-nm Source-Drain Separation with use of Shadow Deposition Techniques: Toward Faster, More Sensitive Molecule-Based Devices

E. Tracy Turner Jones, Oliver M. Chyan, and Mark S. Wrighton*

Department of Chemistry
Massachusetts Institute of Technology
Cambridge, Massachusetts 02139

Received April 14, 1987

We report preparation and characterization of the molecule-based transistor in Figure 1a having a significantly smaller (~50 nm vs. 1.5 μm) source-drain separation and smaller (10^{-14} vs. 10^{-12} mol) amount of redox polymer comprising the channel compared to previously reported[1] devices like that in Figure 1b. The new microstructure with 50-nm source-drain spacing can be prepared by shadow deposition techniques[2] avoiding the need for X-ray[3] or e^- beam[4] lithography. The 50-nm spacing for the open-faced sandwich structure rivals the smallest spacing achievable with conventional sandwich arrangements of electrode/polymer/electrode used to demonstrate the first "bilayer" assemblies.[5]

Figure 2 shows the sequence used to prepare the new microstructure in Figure 1a. The procedure begins with a Si_3N_4-coated

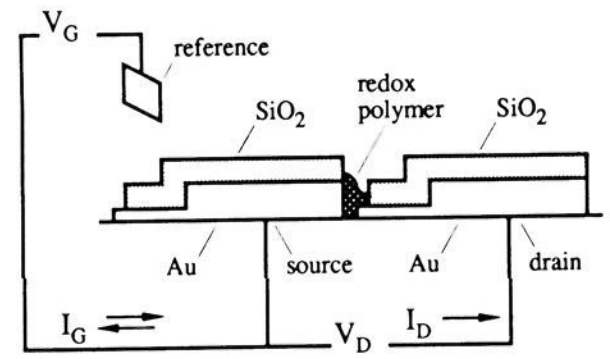

Figure 1. (a) Device structure reported here and (b) previously.[1d]

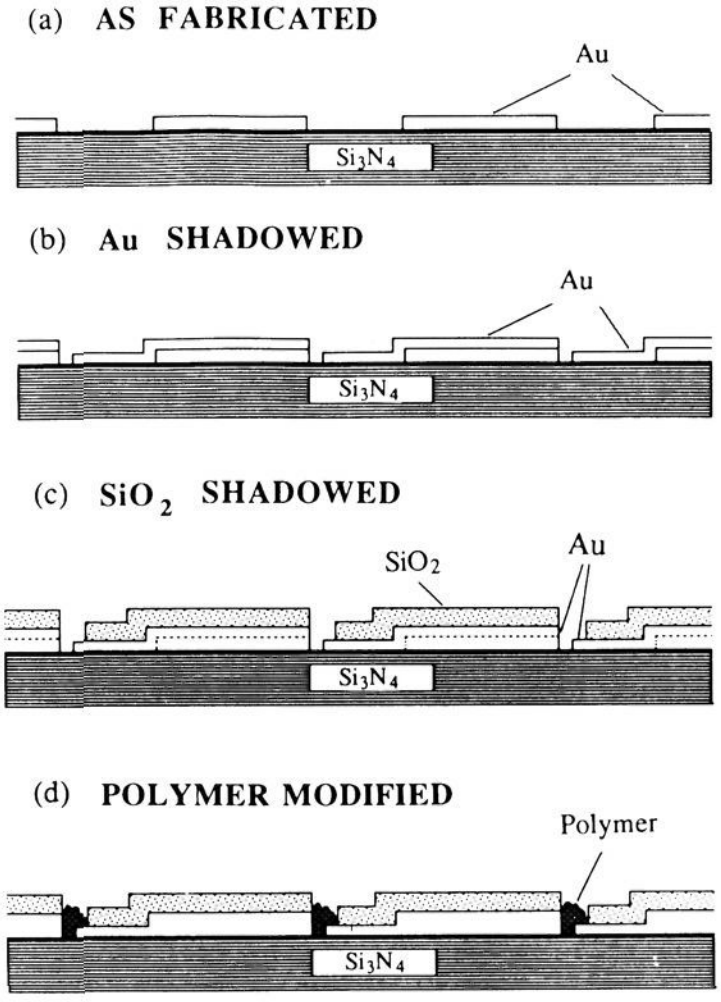

Figure 2. Fabrication sequence for a 50-nm device.

Si wafer of microelectrode arrays previously described.[1a] Each chip on the wafer consists of eight, individually addressable Au microelectrodes each ~50 μm long × 2.5 μm wide × 0.1 μm thick with spacings between microelectrodes of ~1.5 μm. The first step involves a line of sight e^- beam deposition of 50 nm of Au onto the wafer at an angle α as illustrated in Figure 3. Generally, prior to Au deposition 5 nm of Cr is deposited as an adhesion layer. The line of sight deposition of Au results in a larger (~4 μm wide) microelectrode than the original (2.5 μm wide), but the spacing can be closed to 50–100 nm as established by scanning electron microscopy (SEM), Figure 4. Variation of α gives rise to variation in the spacing in a manner consistent with the length of the expected shadow. From SEM it is evident that imperfections on the edges of the original microelectrodes give rise to uneven

(1) (a) Kittlesen, G. P.; White, H. S.; Wrighton, M. S. *J. Am. Chem. Soc.* **1984**, *106*, 7389. (b) Paul, E. W.; Ricco, A. J.; Wrighton, M. S. *J. Phys. Chem.* **1985**, *89*, 1441. (c) Thackeray, J. W.; White, H. S.; Wrighton, M. S. *J. Phys. Chem.* **1985**, *89*, 5133. (d) Lofton, E. P.; Thackeray, J. W.; Wrighton, M. S. *J. Phys. Chem.* **1986**, *90*, 6080.

(2) (a) Dean, R. H.; Matarese, R. J. *IEEE Trans. Electron Devices* **1975**, *ED-22*, 358. (b) Dolan, G. J. *Appl. Phys. Lett.* **1977**, *31*, 337. (c) Speidell, J. L. *J. Vac. Sci. Technol.* **1981**, *19*, 693. (d) Holdeman, L. B.; Barber, R. C.; Abita, J. L. *J. Vac. Sci. Technol.* **1985**, *B3*, 956.

(3) (a) Flanders, D. C. *Appl. Phys. Lett.* **1980**, *36*, 93. (b) Chou, S. Y.; Smith, H. I.; Antoniadis, D. A. *J. Vac. Sci. Technol.* **1985**, *B3*, 1587. (c) Smith, H. I. *J. Vac. Sci. Technol.* **1986**, *B4*, 148.

(4) (a) Crewe, A. V. *J. Vac. Sci. Technol.* **1979**, *16*, 255. (b) Howard, R. E.; Hu, E. L.; Jackel, L. D.; Grabbe, P.; Tennant, D. M. *Appl. Phys. Lett.* **1980**, *36*, 592. (c) Dix, C.; Flavin, P. G.; Hendy, P.; Jones, M. E. *J. Vac. Sci. Technol.* **1985**, *B3*, 131. (d) Emoto, F.; Gamo, K.; Namba, S.; Samoto, N.; Shimizu, R. *Jpn. J. Appl. Phys.* **1985**, *24*, L809.

(5) (a) Pickup, P. G.; Murray, R. W. *J. Am. Chem. Soc.* **1983**, *105*, 4510. (b) Pickup, P. G.; Leidner, C. R.; Denisevich, P.; Murray, R. W. *J. Electroanal. Chem.* **1984**, *164*, 39. (c) Pickup, P. G.; Kutner, W.; Leidner, C. R.; Murray, R. W. *J. Am. Chem. Soc.* **1984**, *106*, 1991. (d) Morishima, Y.; Fukushima, Y.; Nozakura, S. *J. Chem. Soc., Chem. Commun.* **1985**, *13*, 912. (e) Elliott, C. M.; Redepenning, J. G.; Balk, E. M. *J. Electroanal. Chem.* **1986**, *213*(*2*), 203. (f) Chidsey, C. E. D.; Murray, R. W. *Science (Washington, DC)* **1986**, *231*, 25.

0002-7863/87/1509-5526$01.50/0

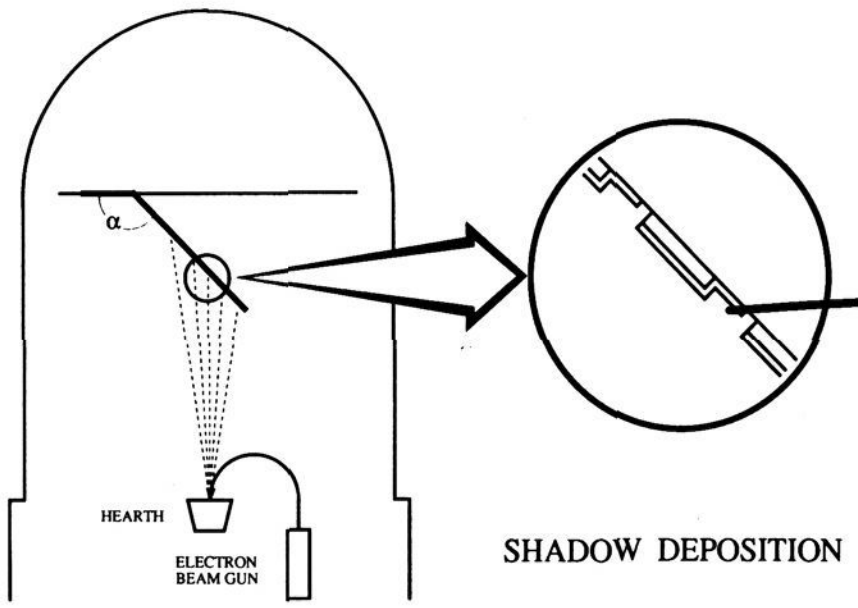

Figure 3. Shadow deposition apparatus.

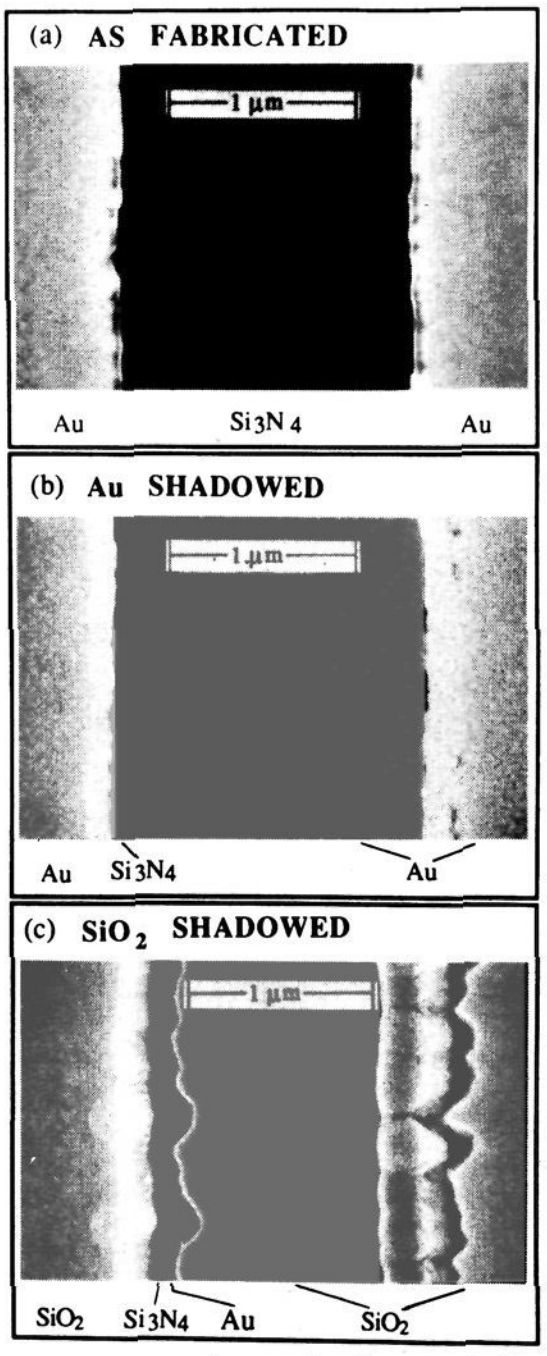

Figure 4. Scanning electron micrographs of a pair of microelectrodes at different stages of the fabrication sequence, Figure 2. (a) Original microelectrodes with 1.5 μm spacing. (b) Gap closed to 50–70 nm by shadow deposition of Cr and Au. (c) Electroactive area of previously widened microelectrodes reduced upon shadow deposition of insulating SiO_2 layer. Uneven spacing reflects original imperfections on the edge of the left microelectrode.

spacings between the microelectrodes after shadow deposition. Indeed, the shadows accurately "image" the imperfections in a straightforward manner. Spacings cited here are "average" values.

The larger microelectrodes formed by shadow deposition of Au have the disadvantage that the absolute amount of electroactive area is relatively large. When redox material is electrochemically deposited, a device results that involves a much larger amount

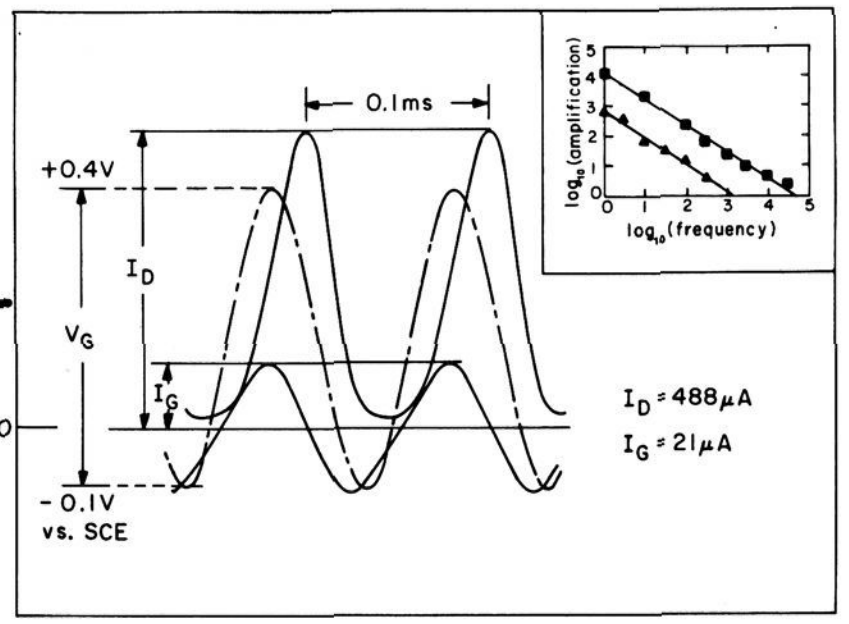

Figure 5. Gate potential (V_G), gate current (I_G), and drain current (I_D) at 10 kHz for an ultrasmall gap polyaniline-based transistor, drain voltage V_D = 100 mV. Inset shows $\log_{10}$ (amplification) vs. $\log_{10}$ (frequency) of 1.5 μm gap (▲) vs. 70 nm gap (■) polyaniline-based transistor, Figure 1. Blank experiments (no polyaniline on microelectrodes) show that the I_G and I_D measured for the polyaniline-based device are principally (>99%) due to oxidation/reduction and resulting changes in conductivity of polyaniline.

of active material than required to span the 50-nm spacing. A second shadow deposition process, Figure 2, line of sight e^- beam deposition of 100 nm of SiO_2 at an angle ∝ smaller than for the Au deposition step, covers the majority of the exposed Au with an insulator, Figure 4. The result is a set of closely spaced (50–100 nm) microelectrodes with ultrasmall electrode areas. The total microelectrode area available depends on the original microelectrode thickness, ∝ for SiO_2 deposition, and the thickness of the shadow deposited Au. Typical area available is estimated to be below 10^{-7} cm^2 per microelectrode. Figure 4 includes SEM showing a closely spaced pair of microelectrodes that is the product of the shadow deposition of Au followed by SiO_2. Electrochemical deposition of $(BPQ^{2+/+})_n$,[6] from *N,N'-bis*(*p*-trimethoxysilylbenzyl)-4,4'-bipyridinium, or polyaniline[1d,7] onto the microfabricated structure shows that the SiO_2 is an effective insulator and that the exposed Au is electrochemically active. SEM establishes the polymer to be deposited mainly in the 50-nm channel region as in Figure 1a. Electrochemical characterization of the system shows that the amount of polymer needed to make a connection between two microelectrodes is $<10^{-14}$ mol of BPQ^{2+} units as established by the integration of a cyclic voltammogram associated with the $BPQ^{2+} \rightleftarrows BPQ^+$ interconversion for microelectrodes connected by the $(BPQ^{2+/+})_n$ polymer. These data show that 10^{-2} times the amount of $(BPQ^{2+/+})_n$ is needed in comparison to the original microelectrode array.

Smaller microelectrode spacing and smaller polymer volume mean that molecule-based transistors require less energy for switching and can be switched more rapidly.[1d] Polyaniline-based transistors, Figure 1a, with 50–100-nm source-drain separation have been demonstrated to switch from off to maximum on by passing $<10^{-9}$ C, 10^{-2} times the charge needed with the original dimensions.[1d] Figure 5 includes an electrochemical characterization of the polyaniline connecting two microelectrodes in that the I_G vs. V_G is in essence a cyclic voltammogram with a sinusoidal variation in voltage. Figure 5 also reveals the change in conductivity accompanying cyclic oxidation/reduction as reflected in variation in I_D as V_G is varied. The data demonstrate power gain at frequencies exceeding 10 kHz almost 10^2 times higher than for a control device with a 1.5 μm source-drain separation. At

(6) (a) Dominey, R. N.; Lewis, T. J.; Wrighton, M. S. *J. Phys. Chem.* **1983**, *87*, 5345. (b) Lewis, T. J.; White, H. S.; Wrighton, M. S. *J. Am Chem. Soc.* **1984**, *106*, 6947.

(7) (a) Mohilner, D. M.; Adams, R. N.; Argersinger, W. J., Jr. *J. Am. Chem. Soc.* **1962**, *84*, 3618. (b) Jozefowicz, M.; Yu, L. T.; Perichon, J.; Buvet, R. *J. Polym. Sci., Part C* **1969**, *22*, 1187. (c) Diaz, A. F.; Logan, J. A. *J. Electroanal. Chem.* **1980**, *111*, 111.

10 kHz the device turns on to nearly the same extent as at 1 Hz. The polyaniline device shows an easily detected variation in drain current, I_D, for flow of only 10^{-12} C in the gate circuit accompanying ΔV_G in the V_G region of maximum transconductance. Thus, the device can respond to a small fraction of a femtomole (10^{-10} C) of charge.

Acknowledgment. We thank the Office of Naval Research and the Defense Advanced Research Project Agency for partial support of the research. Use of the facilities in the M.I.T. Microsystems Technology Laboratories and the NSF-supported Materials Research Laboratory is also gratefully acknowledged.

The *o*-Methoxyphenol-Pendant Cyclam Complexes. A Novel Molecule Designed for Intramolecular Redox Coupling between Monodentate Catecholate and Metal Ions in an N_4 Macrocycle

Eiichi Kimura,*[1a] Shuzo Joko,[1a] Tohru Koike,[1a] and Mutsuo Kodama[1b]

Department of Medicinal Chemistry
Hiroshima University School of Medicine
Kasumi, Minami-ku, Hiroshima 734, Japan
Department of Chemistry, College of
General Education, Hirosaki University
Bunkyo, Hirosaki 036, Japan
Received November 20, 1986

This paper describes the synthesis and characterization of the *o*-methoxy-pendant cyclam complexes. Synergistic, simultaneous oxidation has been revealed by unusually low potentials at −0.30 V vs. SCE for Fe^{2+}/Fe^{3+} and for *o*-methoxyphenolate.

The coordination chemistry of bidentate catechol ligands (cat^{2-}) has long been a subject of chemical[2-7] as well as biochemical interest.[8] Recently, however, monodentate catecholate ($catH^-$) coordination to Fe^{3+} was proposed as an active intermediate in catechol-cleaving dioxygenases, whereupon the catechol becomes susceptible to O_2 attack.[9,10]

With the intention of exploring the redox coupling between the monodentate catecholate and metal ions, we have designed a new cyclam ligand **1**[11] that strategically places the N_4 macrocycle to

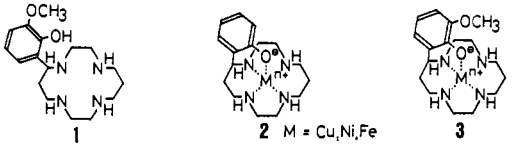

1 2 3

hold metal ions during the course of the redox process close to the *o*-methoxyphenol, an equivalent of catechol.[12] Earlier,[13,14] we reported the X-ray structure[15] of the axial phenolate coordinating complexes (structure **2**), along with the mutually affected redox behavior of the phenolate ion and metal ions.

The new *o*-methoxyphenol-pendant cyclam **1** has pK_a values [determined pH metrically at 25 °C, I = 0.1 M ($NaClO_4$)] of 12.0, 11.16, 8.99 (for phenol, confirmed spectrophotometrically), <2, and <1 and the following UV spectra: λ_{max} 276 nm (ϵ 2500, pH 6.2) for the phenol form; λ_{max} 292 nm (ϵ 4500) and 243 nm (ϵ 8000) for the phenolate form (pH 12.0). In the cyclic voltammogram (CV)[16] of **1**, the anodic oxidation, like *o*-methoxyphenol itself,[17] starts with irreversible 2e oxidative dimethylation to *o*-quinone at +0.58 V (pH 4.0 acetate buffer), +0.45 V (pH 7.3 Tris buffer), and +0.30 V (pH 10.0 carbonate buffer), followed by a reversible[18] *o*-quinone/catechol 2e redox process at +0.33, +0.13, and 0 V, respectively.

Under argon atmosphere[19] **1** forms 1:1 complexes in situ having structure **3** with Ni^{2+} (pH > 7), Cu^{2+} (pH > 9), and Fe^{2+} (pH > 6),[20] as established by pH metric titration. The UV absorptions [λ_{max} 293 nm (ϵ 3600) and 247 nm (ϵ 8600) for Ni^{2+} (pH 8.2), 288 nm (ϵ 5700, *sh*) and 246 nm (ϵ 12000) for Cu^{2+} (pH 10.0), and 287 nm (ϵ 3700) and 243 nm (ϵ 7600) for Fe^{2+} (pH 8.3)], being similar to corresponding features in **2**, support the phenolate coordination in **3**. In electrochemical behavior, the Cu^{2+} complex **3** displays an identical CV (Figure 1-I) with that of the uncoordinated ligand, indicating little influence of Cu^{2+} on oxidation of the axial *o*-methoxyphenolate. Cu^{2+} is not oxidized in the measured potential range.

The CV and RDE of the Ni^{2+} complex **3** Figure 1-II) indicate the 2e oxidation (to **4**) at +0.33 V (pH > 7), followed by 1e

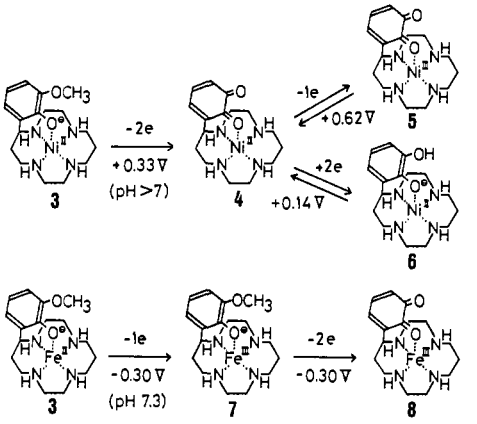

3 4 5 6 3 7 8

(1) (a) Hiroshima University. (b) Hirosaki University.
(2) Pierpont, C. G.; Buchanan, R. M. *Coord. Chem. Rev.* **1981**, *38*, 45-87.
(3) Kessel, S. L.; Emberson, R. M.; Debrunner, P. G.; Hendrickson, D. N. *Inorg. Chem.* **1980**, *19*, 1170-1178, and references therein.
(4) Buchanan, R. M.; Claflin, J.; Pierpont, C. G. *Inorg. Chem.* **1983**, *22*, 2552-2556.
(5) Hartman, J. R.; Foxman, B. M.; Cooper, S. R. *Inorg. Chem.* **1984**, *23*, 1381-1387.
(6) Lynch, M. W.; Hendrickson, D. N.; Fitzgerald, B. J.; Pierpont, C. G. *J. Am. Chem. Soc.* **1984**, *106*, 2041-2049.
(7) deLearie, L. A.; Pierpont, C. G. *J. Am. Chem. Soc.* **1986**, *108*, 6393-6394.
(8) Lee, C.-W.; Ecker, D. J.; Raymond, K. N. *J. Am. Chem. Soc.* **1985**, *107*, 6920-6923, and references therein.
(9) Que, L., Jr.; Lipscomb, J. D.; Münck, E.; Wood, J. M. *Biochim. Biophys. Acta* **1977**, *485*, 60-74. Lauffer, R. B.; Heistand, R. H., II; Que, L., Jr. *J. Am. Chem. Soc.* **1981**, *103*, 3947-3949.
(10) Funabiki, T.; Mizoguchi, A.; Sugimoto, T.; Tada, S.; Tsuji, M.; Sakamoto, H.; Yoshida, S. *J. Am. Chem. Soc.* **1986**, *108*, 2921-2932.
(11) The new ligand **1** was synthesized as follows: Refluxing methyl 2′-(benzyloxy)-3′-methoxycinnamate and 1,9-diamino-3,7-diazanonane in dry CH_3OH for 3 weeks afforded the 14-membered oxotetraamine (mp 170-171 °C, from CH_3CN in 20% yield), and reduction of the oxotetraamine with B_2H_6 in tetrahydrofuran yielded the cyclam derivative **1** (mp 106-107 °C, from CH_3CN in 60% yield).
(12) We have previously synthesized the catechol-pendant cyclam (ref 14); the metal interactions were more complex due to the ligand's rapid decomposition in air.
(13) Kimura, E.; Koike, T.; Takahashi, M. *J. Chem. Soc., Chem. Commun.* **1985**, 385-386.
(14) Kimura, E. *Pure Appl. Chem.* **1986**, *58*, 1461-1466.
(15) X-ray crystal structure of Ni^{2+}-phenolate-pendant-cyclam complex: Iitaka, Y.; Koike, T.; Kimura, E. *Inorg. Chem.* **1986**, *25*, 402-404. X-ray crystal structure of Cu^{2+}-phenolate-pendant-cyclam complex: Kimura, E.; Koike, T.; Uenishi, K.; Hediger, M.; Joko, S.; Arai, Y.; Kodama, M.; Iitaka, Y. *Inorg. Chem.* **1987**, in press.
(16) Electordes used in CV and RDE (rotating disk electrode voltammogram) are all glassy carbons which should be well-polished before every measurement, which were checked by using a reversible redox system of $Ni^{2+,3+}$-cyclam complex in 0.2 M Na_2SO_4 at 25 °C.
(17) Dryhurst, G.; Kadish, K. M.; Scheller, F.; Renneberg, R. *Biological Electrochemistry*; Academic Press: New York, 1982; Vol. 1, pp 116-179.
(18) Reversibility in this and the following redox systems in 0.2 M Na_2SO_4 was checked by log plots of $\log[i/(i_d - i)]$ against the dc potential being invariably linear with reciprocal slope of 30 mV, which corresponds to a reversible two-electron oxidation.
(19) In this and the following electrochemical studies, O_2 is rigorously excluded by using a stream of argon prepurified with an alkaline pyrogallol solution.
(20) Due to rapid decomposition, isolation of these complexes was unsuccessful, except for the pink (high-spin) Ni^{2+} complex (with very low yield) out of a pH 8 aqueous solution of $NiCl_2$ and **1** under argon atmosphere. Anal. Calcd for $C_{17}H_{29}N_4O_2NiCl\cdot H_2O$: C, 47.09; H, 7.21; N, 12.92. Found: C, 47.05; H, 7.40; N, 12.50. The Ni^{2+} complex isolated has shown identical solution behaviors as the one prepared in situ.

0002-7863/87/1509-5528$01.50/0